Vibroacoustic response of an immersed stiffened multilayered shell excited by a plane wave

M. Dana[1], L. Maxit[2]
Laboratoire Vibrations-Acoustique (LVA), INSA Lyon
25 bis, av. Jean Capelle
69621 Villeurbanne, France

J. Bernard[3]
Thales Underwater Systems
525 Route des Dolines
06560 Valbonne, France

ABSTRACT

The modelling of the vibroacoustic response of a periodically rib-stiffened cylindrical multilayered shell is of great interest in numerous industrial applications, among which submarine acoustics. An approach is proposed in this paper to couple an immersed multilayered shell model with models of the axisymmetric stiffeners. The multilayered shell may be modeled either with the transfer matrix method (TMM) or with the direct global method (DGM). Both methods are spectral: displacements and stress are obtained in the wavenumber domain before reconstructing the solution in the physical domain. This allows us representing different types of layers: isotropic, orthotropic, fluid, etc. The stiffeners are coupled to the multilayered shell at the internal radius of the latter. They are introduced in the formulation by dynamic circumferential admittances which are estimated by classic finite element methods. To illustrate the method we'll present different results as much for validation as for comparison with the unstiffened shell.

Keywords: Sound, Insulation, Transmission

1. INTRODUCTION

In military naval industry, designing submarines antennas is of great complexity, especially the flank antennas for which to determine an accurate signal response is of crucial interest. A reliable configuration for modeling such a problem is to consider a cylindrical multilayered structure reinforced at its inner radius by a periodic stiffeners array, and excited by an incident plane wave at its outer radius.
This article aims to develop an analytical method for the coupling of the stiffeners to the multilayered structure and to reconstruct the pressure field at the antenna radius via substructuring approach.

[1]email: maxime.dana1@gmail.com
[2]email: laurent.maxit@insa-lyon.fr
[3]email: Julien.Bernard@fr.thalesgroup.com

Many spectral methods already cover the problem of modeling the unribbed structure excited by a plane wave [1–5], and always rely on the same principle: first one has to solve the problem in each layer of the structure, then one has to find a way of assembly the whole system in order to represent the multilayered structure behaviour. Two of them are investigated in this article: Helmholtz decomposition [1] coupled to direct global matrix [2]; numerical integration of state-space equation coupled to transfer matrix method [3–5]. First method is limited to isotropic layers while solid layers can be chosen either orthotropic in the second. However, the latter suffers great instability when considering finite fluid layers.
The coupling with the stiffeners array must adapt to either modeling method described above.
The substructuring approach used to solve the full problem is detailed in Sec. 2. In Sec. 3 and Sec. 4 we calculate the response of the subsystems.
The coupling between both subsystems is detailed in Sec. 5.
Finally we present validation results for the transfer matrix method in Sec. 6.

2. PRESENTATION OF THE PROBLEM

2.1. Global system

To switch between physical and spectral domains, the Fourier transform (1) is defined below.

$$\begin{aligned} F(r,\phi,z) &= \frac{1}{2\pi}\sum_{-\infty}^{+\infty} e^{in\phi}\int_{-\infty}^{+\infty}\tilde{F}(r,n,\alpha)e^{i\alpha z}d\alpha \\ \tilde{F}(r,n,\alpha) &= \frac{1}{2\pi}\int_{0}^{2\pi} e^{-in\phi}\int_{-\infty}^{+\infty}F(r,\phi,z)e^{-i\alpha z}dzd\phi \end{aligned} \tag{1}$$

Let us consider an infinite multilayered cylindrical structure (MCS) centered on the z axis as shown in Fig.1. The first layer is assumed to be a steel shell, and the other layers are various coatings stacked upon it. The structure is reinforced by a periodic stiffeners array (PSA) of equal spacing d, which connects to the steel shell at its inner radius r_0. It is excited by a unit incident plane wave at the outer radius r_N, its polar angle is noted ϕ_i.

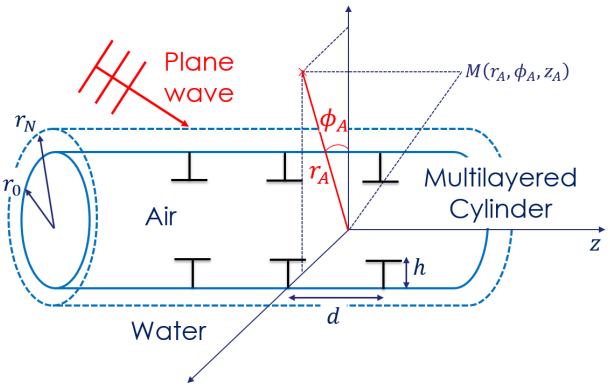

Figure 1: Multilayered cylindrical shell (MCS) reinforced by periodic stiffeners array (PSA)

Layers are numbered from 1 to N starting from the steel shell. 0 and $N+1$ are respectively the internal cavity filled with air and the semi-infinite exterior medium filled by water.
Displacements and stresses in any layer j are noted $\boldsymbol{u}_j = (u_{jz}\ u_{j\phi}\ u_{jr})^T$ and $\boldsymbol{\sigma}_j = (\sigma_{j,rz}\ \sigma_{j,r\phi}\ \sigma_{j,rr})^T$.

A punctual sensor is placed into the external fluid, at a radius r_A.
To determine the acoustic radiation of such structure at the sensor location, a classic substructuring approach is used and detailed below.

2.2. Substructuring approach and superposition principle

A substructuring approach is chosen. The reinforced multilayered global structure is split into two separate subsystems, the unribbed MCS (SS1) and the PSA (SS2) [8, 9]. This is represented in Fig. 2:

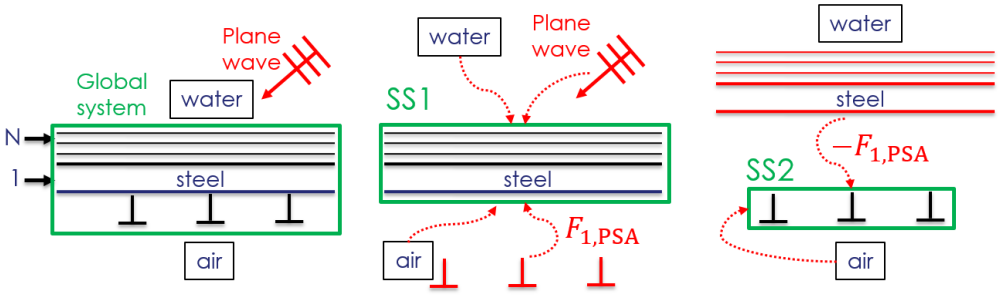

(a) Global system (b) Loads applied on SS1 (c) Loads applied on SS2

Figure 2: Substructuring approach and superposition principle

Applying the superposition principle on subsystem SS1 entails the equivalence between determining its response to both external and internal loads and getting the one from the reinforced fluid-loaded MCS global system to a plane wave excitation.

Besides, the principle of reciprocal actions states that load $\boldsymbol{\sigma}^{\text{INT}}_{1,\text{MCS}}$ applied by subsystem SS2 on subsystem SS1 at coupling attachment points is the opposite of the one exerted on subsystem SS2 by subsystem SS1.
From fluid-loaded subsystem SS1, plane wave excitation is an external load, while reaction of the PSA is an internal load.

Then displacement and stress fields at the inner radius, respectively $\boldsymbol{u}_1$ and $\boldsymbol{\sigma}_1$, as well as stress field at the outer radius $\boldsymbol{\sigma}_N$ can be written as follows:

$$\boldsymbol{u}_1(r_0, n, \alpha) = \boldsymbol{u}^{\text{EXT}}_{1,\text{MCS}}(r_0, n, \alpha) + \boldsymbol{u}^{\text{INT}}_{1,\text{MCS}}(r_0, n, \alpha) \tag{2}$$

$$\boldsymbol{\sigma}_1(r_0, n, \alpha) = \boldsymbol{\sigma}^{\text{INT}}_{1,\text{MCS}}(r_0, n, \alpha) + \boldsymbol{\sigma}_{\text{fli}}(r_0, n, \alpha) \tag{3}$$

$$\boldsymbol{\sigma}_N(r_N, n, \alpha) = \boldsymbol{\sigma}^{\text{EXT}}_{N,\text{MCS}}(r_N, n, \alpha) + \boldsymbol{\sigma}_{\text{fle}}(r_N, n, \alpha) \tag{4}$$

- When external load is applied on SS1 at its outer radius r_N, stress field generated at the outer radius is noted $\boldsymbol{\sigma}^{\text{EXT}}_{N,\text{MCS}}$ and no external load is applied at the inner radius.
  Displacement field generated at the inner radius is noted $\boldsymbol{u}^{\text{EXT}}_{1,\text{MCS}}$ (see Fig. 2(b)).

- When internal load is applied on SS1, displacement field at the inner radius is noted $\boldsymbol{u}^{\text{INT}}_{1,\text{MCS}}$ while the surface reaction of the PSA on the MCS is noted $\boldsymbol{\sigma}^{\text{INT}}_{1,\text{MCS}}$.
  No internal load is applied at the outer radius (see Fig. 2(c)).

- When external and internal loads apply on SS1, air in the cavity and water surrounding the MCS apply reaction stresses at inner and outer radius, noted respectively $\boldsymbol{\sigma}_{\text{fli}}$ and $\boldsymbol{\sigma}_{\text{fle}}$.

3. RESPONSE OF SUBSYSTEM SS1

In this section we describe how to get the response of the fluid-loaded subsystem SS1 for each spectral method retained for the modeling of the MCS. We explicit external load as fluid reaction stresses in this section, and the internal load is explained in the next section.

3.1. External load and fluid reaction stresses

External load applied on SS1 is the incident plane wave excitation at the outer radius, to which induced loadings of external and internal fluids must be added. The incident wavenumber is noted α_0^i.
Such a scattering problem is commonly dealt with by decomposing the total spectral pressure in the water as the sum of the blocked pressure p_b and the scattered pressure p_e [10]. With $\boldsymbol{u}_N$ being the displacement field at the outer radius, these are explicited in (5) below:

$$
\begin{aligned}
& p_T(r,n,\alpha) = p_b(r,n,\alpha) + p_e(r,n,\alpha) \\
& \begin{cases}
p_b(r,n,\alpha) = 2\pi(-i)^n e^{-in\phi_i} \left[J_n(\gamma_{|\alpha_0^i} r) - \dfrac{J_n'(\gamma_{|\alpha_0^i} r_N)}{H_n'(\gamma_{|\alpha_0^i} r_N)} H_n(\gamma_{|\alpha_0^i} r) \right] \delta(\alpha - \alpha_0^i) \\
p_e(r,n,\alpha) = Z_{\text{fle}}(r,n,\alpha) \boldsymbol{u}_N(r_N,n,\alpha) \cdot \boldsymbol{e_r}, \quad Z_{\text{fle}}(r,n,\alpha) = \dfrac{\rho_e \omega^2 H_n(\gamma(\alpha) r)}{\gamma(\alpha) H_n'(\gamma(\alpha) r_N)}
\end{cases}
\end{aligned}
\tag{5}
$$

The compression velocity in the external fluid is c_e, and $\gamma(\alpha) = \sqrt{k^2 - \alpha^2}$ with $k = \dfrac{\omega}{c_e}$.
Stress field $\boldsymbol{\sigma}_{N,\text{MCS}}^{\text{EXT}}$ defined at the outer radius in (4) then becomes explicit:

$$
\begin{aligned}
& \boldsymbol{\sigma}_N(r_N,n,\alpha) = \boldsymbol{\sigma}_{N,\text{MCS}}^{\text{EXT}}(r_N,n,\alpha) + \boldsymbol{\sigma}_{\text{fle}}(r_N,n,\alpha) \\
& \text{with: } \begin{cases}
\boldsymbol{\sigma}_{N,\text{MCS}}^{\text{EXT}}(r_N,n,\alpha) & = -p_b(r_N,n,\alpha)\boldsymbol{e_r} \\
\boldsymbol{\sigma}_{\text{fle}}(r_N,n,\alpha) & = -p_e(r_N,n,\alpha)\boldsymbol{e_r}
\end{cases}
\end{aligned}
\tag{6}
$$

The radiated spectral pressure in the internal fluid is given below [1]:

$$
p_{1i}(r_0,n,\alpha) = Z_{\text{fli}}(r_0,n,\alpha) \boldsymbol{u}_1(r_0,n,\alpha) \cdot \boldsymbol{e_r}, \quad Z_{\text{fli}}(r,n,\alpha) = \frac{\rho_i \omega^2 J_n(\gamma_i(\alpha) r)}{\gamma_i(\alpha) J_n'(\gamma_i(\alpha) r_0)} \tag{7}
$$

The compression waves velocity in the internal fluid is c_i, and $\gamma_i(\alpha) = \sqrt{k_i^2 - \alpha^2}$ with $k_i = \dfrac{\omega}{c_i}$.

Stress field induced at the inner radius by the internal fluid loading is given below:

$$
\boldsymbol{\sigma}_{\text{fli}}(r_0,n,\alpha) = p_{1i}(r_0,n,\alpha)\boldsymbol{e_r} \tag{8}
$$

3.2. Admittance matrices at the SS1-SS2 interface

The coupling between both subsystems SS1 and SS2 requires to introduce two admittance matrices $R^a(n,\alpha)$ and $R^b(n,\alpha)$, which take into account fluid loadings and are defined below:

$$\boldsymbol{u}_{1,\text{MCS}}^{\text{EXT}}(r_0,n,\alpha) = R^a(n,\alpha)\boldsymbol{\sigma}_{N,\text{MCS}}^{\text{EXT}}(r_N,n,\alpha) \tag{9}$$

$$\boldsymbol{u}_{1,\text{MCS}}^{\text{INT}}(r_0,n,\alpha) = R^b(n,\alpha)\boldsymbol{\sigma}_{1,\text{MCS}}^{\text{INT}}(r_0,n,\alpha) \tag{10}$$

Admittance matrix R^a connects displacement field $\boldsymbol{u}_{1,\text{MCS}}^{\text{EXT}}$ of the steel shell at the coupling interface with the plane wave excitation load $\boldsymbol{\sigma}_{N,\text{MCS}}^{\text{EXT}}$ applied at the outer radius.
Admittance matrix R^b connects displacement field $\boldsymbol{u}_{1,\text{MCS}}^{\text{INT}}$ of the steel shell at the coupling interface with internal load applied at the inner radius $\boldsymbol{\sigma}_{1,\text{MCS}}^{\text{INT}}$.

Eqn. 2 can then be detailed as follows:

$$\boldsymbol{u}_1(r_0,n,\alpha) = R^a(n,\alpha)\boldsymbol{\sigma}_{N,\text{MCS}}^{\text{EXT}}(r_N,n,\alpha) + R^b(n,\alpha)\boldsymbol{\sigma}_{1,\text{MCS}}^{\text{INT}}(r_0,n,\alpha) \tag{11}$$

3.3. Transfer matrix method (TMM)

3.3.1. Principle

For more details on the TMM, one can refer to [6].
Here we only introduce the relation one can get between the hybrid state vector evaluated at both ends of the MCS:

$$\begin{pmatrix}\boldsymbol{u}_N\\ \boldsymbol{\sigma}_N\end{pmatrix}(r_N,n,\alpha) = \begin{pmatrix}T_{\boldsymbol{u}_N\boldsymbol{u}_1} & T_{\boldsymbol{u}_N\boldsymbol{\sigma}_1}\\ T_{\boldsymbol{\sigma}_N\boldsymbol{u}_1} & T_{\boldsymbol{\sigma}_N\boldsymbol{\sigma}_1}\end{pmatrix}(n,\alpha)\begin{pmatrix}\boldsymbol{u}_1\\ \boldsymbol{\sigma}_1\end{pmatrix}(r_0,n,\alpha) \tag{12}$$

Submatrices in system (12) constitute the transfer matrix of the whole structure, established by multiplying the different transfer matrices of elementary layers in the MCS. Developments for getting the global transfer matrix are available in [6].

3.3.2. Displacement field at the inner radius

Closing the matrix system (12) with (6) and (8) leads to explicit expressions for admittance matrices R^a and R^b:

$$\begin{cases} R^a(n,\alpha) = X^{-1}(n,\alpha)\\ R^b(n,\alpha) = (R^aY)(n,\alpha)\\ X(n,\alpha) = -\left[T_{\text{fle}|r_N}T_{\boldsymbol{u}_N\boldsymbol{u}_1} + T_{\boldsymbol{\sigma}_N\boldsymbol{u}_1} + \left(T_{\boldsymbol{\sigma}_N\boldsymbol{\sigma}_1} + T_{\text{fle}|r_N}T_{\boldsymbol{u}_N\boldsymbol{\sigma}_1}\right)T_{\text{fli}|r_0}\right](n,\alpha)\\ Y(n,\alpha) = \left[T_{\boldsymbol{\sigma}_N\boldsymbol{\sigma}_1} + T_{\text{fle}|r_N}T_{\boldsymbol{u}_N\boldsymbol{\sigma}_1}\right](n,\alpha)\end{cases} \tag{13}$$

with T_{fli} and T_{fle} being derived from fluid impedances Z_{fli} and Z_{fle}:

$$\begin{cases} T_{\text{fli}}(r,n,\alpha) = Z_{\text{fli}}(r,n,\alpha)\boldsymbol{e_r}\otimes\boldsymbol{e_r}\\ T_{\text{fle}}(r,n,\alpha) = Z_{\text{fle}}(r,n,\alpha)\boldsymbol{e_r}\otimes\boldsymbol{e_r}\end{cases} \tag{14}$$

3.3.3. Pressure field at the sensor radius

Once the internal load is made explicit, one can reconstruct the displacement field in the last coating at the outer radius $\boldsymbol{u}_N(r_N, n, \alpha)$ by using the first equation of the matrix system (12):

$$\boldsymbol{u}_N(r_N, n, \alpha) = T_{\boldsymbol{u}_N\boldsymbol{u}_1}(n, \alpha)\boldsymbol{u}_1(r_0, n, \alpha) + T_{\boldsymbol{u}_N\boldsymbol{\sigma}_1}(n, \alpha)\boldsymbol{\sigma}_1(r_0, n, \alpha) \tag{15}$$

The pressure field can then be obtained with the relation (5).

3.4. Direct global method (DGM)

3.4.1. Principle

The DGM relies on a Helmholtz decomposition of displacement and stress fields inside each elementary layer of the MCS [1, 2]. Displacements and stresses in a layer are connected to the Helmholtz decomposition coefficients with elementary matrices. These are then used to assembly a global matrix by expressing the continuity conditions between layers. Fluid and solid layers are assumed respectively perfect and isotropic.

More details on the global matrix method can be found in [6].

3.4.2. Displacement field at the inner radius

Let us consider mechanical point excitations F_m^a and F_m^b applied respectively at outer and inner radius r_0 and r_N chosen unitary in spectral domain:

$$\begin{aligned} F_m^a(r_N, n, \alpha) &= 1 \cdot \boldsymbol{e_m} \\ F_m^b(r_0, n, \alpha) &= 1 \cdot \boldsymbol{e_m} \end{aligned} \tag{16}$$

with $\boldsymbol{e_m}$ being any of the three cylindrical base vectors $\boldsymbol{e_z}$, $\boldsymbol{e_\phi}$ ou $\boldsymbol{e_r}$.

Displacement fields generated at the inner radius for each of the excitations described in (16) are:

$$\begin{aligned} \left(\boldsymbol{e_m} = \boldsymbol{e_z} \iff F_z^a/F_z^b \text{ imposed}\right) &\rightsquigarrow \boldsymbol{u}_{1|F_z^a}/\boldsymbol{u}_{1|F_z^b} \\ \left(\boldsymbol{e_m} = \boldsymbol{e_\phi} \iff F_\phi^a/F_\phi^b \text{ imposed}\right) &\rightsquigarrow \boldsymbol{u}_{1|F_\phi^a}/\boldsymbol{u}_{1|F_\phi^b} \\ \left(\boldsymbol{e_m} = \boldsymbol{e_r} \iff F_r^a/F_r^b \text{ imposed}\right) &\rightsquigarrow \boldsymbol{u}_{1|F_r^a}/\boldsymbol{u}_{1|F_r^b} \end{aligned} \tag{17}$$

Each column of admittance matrices R^a and R^b are identical to the displacement fields introduced in (17) for excitations have been chosen unitary:

$$\begin{aligned} R^a(n, \alpha) &= \left(\boldsymbol{u}_{1|F_z^a} \middle| \boldsymbol{u}_{1|F_\phi^a} \middle| \boldsymbol{u}_{1|F_r^a} \right) \\ R^b(n, \alpha) &= \left(\boldsymbol{u}_{1|F_z^b} \middle| \boldsymbol{u}_{1|F_\phi^b} \middle| \boldsymbol{u}_{1|F_r^b} \right) \end{aligned} \tag{18}$$

Each displacement field requires a DGM calculation, for which the mechanical excitation of (16) changes.

3.4.3. Pressure field at the sensor radius

Once the PSA reaction load $\boldsymbol{\sigma}^{\text{INT}}_{1,\text{MCS}}(r_0, n, \alpha)$ is made explicit (see next section), one last DGM calculation enables to compute the response for the global system.
By reconstructing the displacement field in the last coating at the outer radius $u_N(r_N, n, \alpha)$, one can get the spectral total pressure at the sensor radius located in the semi-infinite fluid medium.

4. RESPONSE OF SUBSYSTEM SS2

In this section we explain how to model the response of subsystem SS2 to an excitation applied at the shell/ribs interface Detail on how each stiffener of the PSA is modeled is given below.

4.1. Finite element modeling of the stiffeners

Each of the axisymmetrical stiffeners of the PSA is modeled by shell elements, which implies taking into account 4 degrees of freedom at each node of the mesh represented in Fig. 3 :

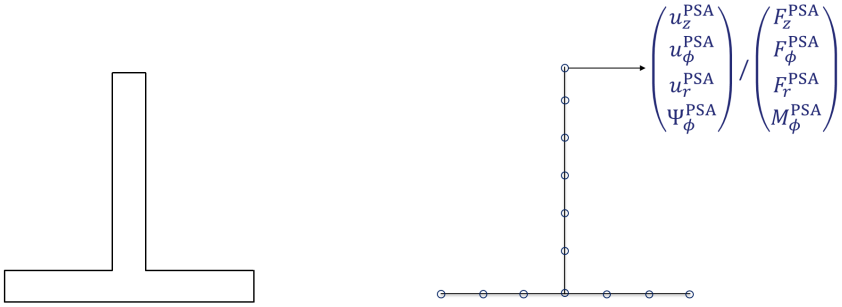

(a) Rib geometry (b) Shell elements modeling

Figure 3: Modeling of any stiffener

At cylinder attachment points $(r_0, z = qd)$, one can define for any stiffener the dynamic stiffness matrix $[B(n)]$ connecting degrees of freedom and loads by:

$$[B(n)] \begin{pmatrix} u_z^{\text{PSA}} \\ u_\phi^{\text{PSA}} \\ u_r^{\text{PSA}} \\ \Psi_\phi^{\text{PSA}} \end{pmatrix} (r_0, n, z = qd) = \begin{pmatrix} F_z^{\text{PSA}} \\ F_\phi^{\text{PSA}} \\ F_r^{\text{PSA}} \\ M_\phi^{\text{PSA}} \end{pmatrix} (r_0, n, z = qd) \tag{19}$$

where loads in the right hand side of (19) are series harmonics of forces per unit length along the circumferential direction $\left(F_z^{\text{PSA}}, F_\phi^{\text{PSA}}, F_r^{\text{PSA}}, M_\phi^{\text{PSA}}\right)^T (r_0, \phi, z)$, acting on the PSA at cylinder attachment points.
We specify that air loading on the stiffeners is neglected when calculating the matrices $[B(n)]$.

5. COUPLING SUBSYSTEMS SS1 AND SS2

5.1. Extending the MCS fields at the inner radius

The PSA introduces at coupling attachment points a rotation around the cicumferential axis, whose angle is noted Ψ_ϕ^{PSA}, and verifies the relationship:

$$\Psi_\phi^{\text{PSA}}(r_0,\phi,z) = \frac{\partial u_r^{\text{PSA}}}{\partial z}(r_0,\phi,z) \tag{20}$$

Besides, the meridional moment per surface unit M_ϕ^{PSA} introduced by the rotation angle is assumed to be equivalent to the following radial excitation force [1]:

$$F_r^{\text{PSA}}(r_0,\phi,z) = -\frac{\partial M_\phi^{\text{PSA}}}{\partial z}(r_0,\phi,z) \tag{21}$$

Therefore displacements and stresses at the inner radius must be extended to this new degree of freedom to achieve the coupling between subsystems SS1 and SS2.

Besides, admittance matrices defined in (9)-(10) are extended as well using (20)-(21) [1]:

$$M(n,\alpha) = \begin{pmatrix} M_{11} & M_{12} & M_{13} & M_{14} \\ M_{21} & M_{22} & M_{23} & M_{24} \\ M_{31} & M_{32} & M_{33} & M_{34} \\ M_{41} & M_{42} & M_{43} & M_{44} \end{pmatrix} \tag{22}$$

$$\text{with: } \begin{cases} M_{14}(n,\alpha) = -i\alpha M_{13}(n,\alpha), & M_{41}(n,\alpha) = i\alpha M_{31}(n,\alpha) \\ M_{24}(n,\alpha) = -i\alpha M_{23}(n,\alpha), & M_{42}(n,\alpha) = i\alpha M_{32}(n,\alpha) \\ M_{34}(n,\alpha) = -i\alpha M_{33}(n,\alpha), & M_{43}(n,\alpha) = i\alpha M_{33}(n,\alpha) \\ & M_{44}(n,\alpha) = \alpha^2 M_{33}(n,\alpha) \end{cases}$$

with matrix M being either R^a or R^b.

From now on, we consider the displacement and stress fields at the inner radius extended to the fourth degree of freedom, as well as for the admittance matrices.

5.2. Reaction load from subsystem SS2 on subsystem SS1

Internal reaction load applied by subsystem SS2 on subsystem SS1 is found by applying the principle of reciprocal actions:

$$\begin{aligned} \boldsymbol{\sigma}_{1,\text{MCS}}^{\text{INT}}(r_0,n,z) &= -\sum_{q=-\infty}^{\infty} \begin{pmatrix} F_z^{\text{PSA}} \\ F_\phi^{\text{PSA}} \\ F_r^{\text{PSA}} \\ M_\phi^{\text{PSA}} \end{pmatrix} (r_0,n,z=qd)\delta(z-qd) \\ &= -\left[B(n)\right] \sum_{q=-\infty}^{\infty} \boldsymbol{u}_1(r_0,n,z=qd)\delta(z-qd) \end{aligned} \tag{23}$$

The loads per unit length are converted into a reaction force per surface unit for the delta function has dimension $[m^{-1}]$. Internal load $\boldsymbol{\sigma}_{1,\text{MCS}}^{\text{INT}}$ is then homogeneous to a surface pressure.

Fourier transform along the axial direction and use of the Poisson relation entails:

$$\boldsymbol{\sigma}^{\text{INT}}_{1,\text{MCS}}(r_0,n,\alpha) = -\frac{1}{d}\left[B(n)\right]\sum_{q=-\infty}^{\infty}\boldsymbol{u}_1\left(r_0,n,\alpha+\frac{2\pi q}{d}\right) \tag{24}$$

Replacing (24) into (11) leads to:

$$\boldsymbol{u}_1(r_0,n,\alpha) = R^a(n,\alpha)\boldsymbol{\sigma}^{\text{EXT}}_{N,\text{MCS}}(r_N,n,\alpha) - \frac{1}{d}R^b(n,\alpha)\left[B(n)\right]\sum_{q=-\infty}^{\infty}\boldsymbol{u}_1\left(r_0,n,\alpha+\frac{2\pi q}{d}\right) \tag{25}$$

Therefore one can determine the quantity $\sum_{q=-\infty}^{\infty}\boldsymbol{u}_1\left(r_0,n,\alpha+\frac{2\pi q}{d}\right)$ and establish the following expression for the PSA reaction pressure:

$$\begin{aligned}\boldsymbol{\sigma}^{\text{INT}}_{1,\text{MCS}}(r_0,n,\alpha) = -\frac{1}{d}\left[B(n)\right]\left[\text{Id}+\frac{1}{d}\left\{\sum_{q=-\infty}^{\infty}R^b\left(n,\alpha+\frac{2\pi q}{d}\right)\right\}\left[B(n)\right]\right]^{-1}\times \\ \sum_{q=-\infty}^{\infty}R^a(n,\alpha+\frac{2\pi q}{d})\boldsymbol{\sigma}^{\text{EXT}}_{N,\text{MCS}}\left(r_N,n,\alpha+\frac{2\pi q}{d}\right)\end{aligned} \tag{26}$$

Then, the displacement field at the inner radius is fully known by introducing (26) into (11), and one can reconstruct the pressure field for either MCS modeling method, using 3.3.3. or 3.4.3..

6. VALIDATION RESULTS FOR THE TRANSFER MATRIX METHOD

In this section we present preliminary results for the full problem computed with the transfer matrix method for modeling the MCS, in the case of an uncoated steel shell.

6.1. Numerical setup

A reduced steel shell ribbed with a periodic stiffeners array has been investigated for numerical computations
Stiffeners are assumed to be of rectangular section. Dimensions of steel shell and PSA are given in Table 1, and are identical to those used in [7].
The dynamic stiffness matrices $[B(n)]$ for any stiffener are precalculated with a finite element computation, in which the three-dimensional deformation of the section is taken into account.
Last row of Table 1 reminds that the infinite series involved in 26 are truncated numerically into finite sums covering the range $[\![-Q;Q]\!]$.

For vibratory results on displacements, the sensor is located either at the inner radius r_0 or the outer radius r_N. For the results on the acoustic pressure, the sensor is located in the semi-infinite medium at a radius $r_A = 6.04$ cm. Axial position z_A along the shell axis and polar angle ϕ_A are both variable. The incident polar angle of the plane wave is always $\phi_i = 0$.

Following results are compared with an already validated model where a thin shell assumption is made to model the shell.

Table 1: : Numerical setup

Properties	Air	Steel	Water	Stiffener
Density (kg.m^{-3})	1.2 (ρ_i)	7900 (ρ_s)	1000 (ρ_e)	
Sound velocity (m.s^{-1})	340 (c_i)		1470 (c_e)	
Longitudinal velocity (m.s^{-1})		5790 (c_L)		
Transversal velocity (m.s^{-1})		3100 (c_T)		
Inner radius (cm)		4.9 (r_0)		
Outer radius (cm)		5.0 (r_N)		
Stiffeners network period (cm)				1.5 (d)
Height (cm)				0.5 (h)
Width (cm)				0.1
Number of stiffeners Q				10

6.2. Results for displacement fields under normal incidence

First we present vibratory results on the normal displacement field at both inner and outer radius. Comparison to the thin shell model is made with the normal displacement field evaluated at the mid-surface.

6.2.1. Frequency response

Fig. 4 represents the normal displacements as a function of the frequency.
The sensor is placed on a stiffener when $z_A = 0$, and halfway between two consecutive stiffeners when $z_A = \frac{d}{2}$. The observation polar angle is $\phi_A = 0$.

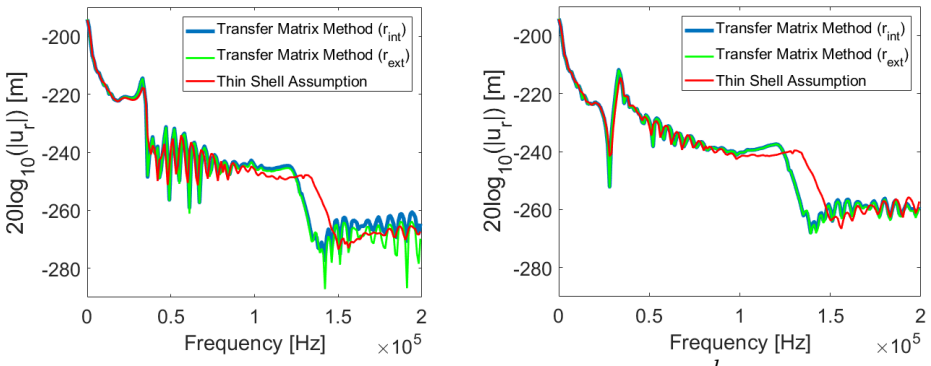

(a) $z_A = 0, \phi_A = 0$ (b) $z_A = \dfrac{d}{2}, \phi_A = 0$

Figure 4: Normal displacement field at inner and outer radius

Both displacement fields are very similar, and one can notice good correlation with the thin shell model at low regime.
One can underline that the correlation of the two responses with the thin shell model fades away with increasing frequency, because the latter is valid only at low frequency.

6.2.2. *Spatial distribution of normal displacements*

In Fig. 5 below we present for a given frequency the normal displacements at both inner and outer radius on the interval $z_A \in [\![-d, d]\!]$ and for $\phi_A \in [\![-\pi, \pi]\!]$.
At low frequencies, good correlation is observed between displacements at the inner or outer radius and those calculated on the mid-surface with the thin shell model, everywhere on the surface of the steel shell.
At higher frequencies, large differences can be observed on Fig. 4(a) and Fig. 4(b) between the developed method and the thin shell model. Below is represented for $f = 133.1$ kHz the spatial variation of displacement field at both inner and outer radius and at the mid-surface:

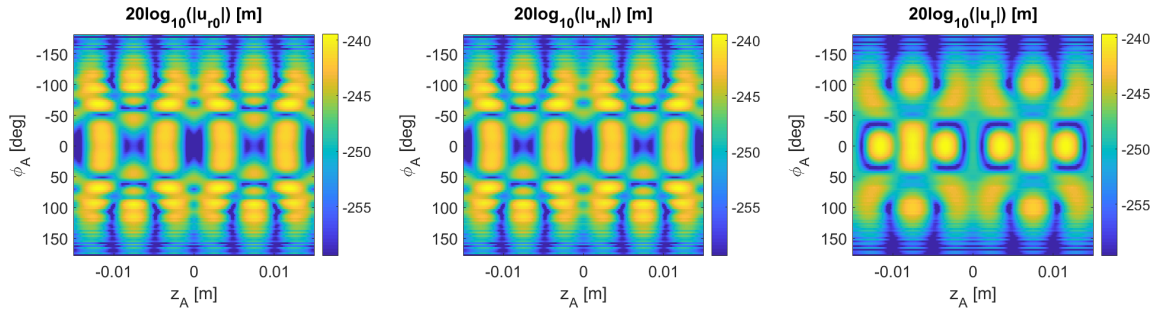

(a) inner radius (b) outer radius (c) mid-surface (thin shell model)

Figure 5: Normal displacement field at $f = 133.1$ kHz

Spatial displacement field at the mid-surface of the equivalent thin shell show large differences with the implemented method.

6.3. Results for acoustic pressure under normal incidence

Now we present acoustic results on the total pressure field evaluated at the sensor radius located in the water, in the case of normal incidence. Comparison to the thin shell model is done again.

In Fig. 6 below are shown two responses according to the frequency, for the same two sensor axial and polar positions considered in Fig. 4:

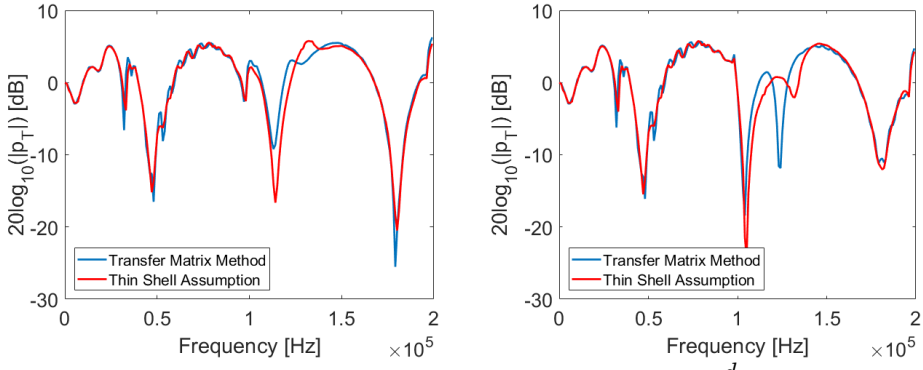

(a) $z_A = 0, \phi_A = 0$ (b) $z_A = \dfrac{d}{2}, \phi_A = 0$

Figure 6: Acoustic total pressure field at $r_A = 6.04$ cm

One can observe the same behaviour than for the normal displacement. Good correlation with the thin shell model is aknowledged at low frequency, then the limitations of the shin shell model induce differences between the responses.

7. CONCLUSION

In this article, we developed a formalism to model cylindrical multilayered ribbed shells. The developed formalism is adaptable to both direct global method or transfer matrix method which shall be retained for modeling the multilayered structure. The preliminary validations exposed in this article shall be followed with much deeper investigation, in particular a cross validation between the direct global method and the transfer matrix method, as well as a comparison between these last two with a finite element method.

REFERENCES

[1] E.A. Skelton, J.H. James, Theoretical acoustics of underwater structures, *Imperial College Press* (1997).

[2] D.C. Ricks, H. Schmidt, A numerically stable global matrix method for cylindrically layered shells excited by ring forces, *J. Acoust. Soc. Am.*, **95** (6), 3339-3349 (1994).

[3] J.R. Fan, Exact theory of strongly thick laminated plates and shells, *Beijing: Science Press* (1996).

[4] W.Q. Chen, Z.G. Bian, H.J. Ding, Three-dimensional vibration analysis of fluid-filled orthotropic FGM cylindrical shells, *International Journal of Mechanical Sciences* **46**, 159-171 (2004).

[5] C. Dutrion, *Étude de faisabilité d'un revêtement élastique pour la furtivité acoustique*, thèse de doctorat-ISAE (2014).

[6] M. Dana, L. Maxit, J. Bernard - Prédiction de la réponse vibro-acoustique de coques cylindriques revêtues immergées, 14 ème Congrès Français d'Acoustique (CFA2018), Le Havre, 23-27 avril 2018.

[7] R. Liétard, D. Décultot and G. Maze, Acoustic scattering from a finite cylindrical shell with evenly spaced stiffeners: Experimental investigation, *J. Acoust. Soc. Am.*, **118**, 2142-2146 (2005).

[8] C.J. Burroughs Acoustic radiation from fluid-loaded in finite circular cylinders with doubly periodic ring supports, *J. Acoust. Soc. Am.*, **75** (3), 715-722 (1984).

[9] L. Maxit Scattering model of a cylindrical shell with internal axisymmetric frames by using the Circumferential Admittance Approach, *Applied Acoustics*, **80** (3), 10-22 (2014).

[10] M.C. Junger, D. Feit, Sound, structures and their interaction. 2nd ed. *Massachusetts Institute of Technology Press* (1986) p. 448